Single-cell, real-time detection of oxidative stress induced in *Escherichia coli* by the antimicrobial peptide CM15

Heejun Choi[a], Zhilin Yang[a], and James C. Weisshaar[a,b,1]

[a]Department of Chemistry and [b]Molecular Biophysics Program, University of Wisconsin, Madison, WI 53706

Edited by James J. Collins, Boston University, Boston, MA, and approved December 8, 2014 (received for review September 15, 2014)

Antibiotics target specific biochemical mechanisms in bacteria. In response to new drugs, pathogenic bacteria rapidly develop resistance. In contrast, antimicrobial peptides (AMPs) have retained broad spectrum antibacterial potency over millions of years. We present single-cell fluorescence assays that detect reactive oxygen species (ROS) in the *Escherichia coli* cytoplasm in real time. Within 30 s of permeabilization of the cytoplasmic membrane by the cationic AMP CM15 [combining residues 1–7 of cecropin A (from moth) with residues 2–9 of melittin (bee venom)], three fluorescence signals report oxidative stress in the cytoplasm, apparently involving O_2^-, H_2O_2, and •OH. Mechanistic studies indicate that active respiration is a prerequisite to the CM15-induced oxidative damage. In anaerobic conditions, signals from ROS are greatly diminished and the minimum inhibitory concentration increases 20-fold. Evidently the natural human AMP LL-37 also induces a burst of ROS. Oxidative stress may prove a significant bacteriostatic mechanism for a variety of cationic AMPs. If so, host organisms may use the local oxygen level to modulate AMP potency.

antimicrobial peptide | oxidative stress | CM15 | real-time ROS assay | *E. coli*

In nature, multicellular organisms produce antimicrobial peptides (AMPs) that participate in the first line of defense against bacterial infection (1). These are ancient molecules that kill a broad, phylogenetically diverse spectrum of bacteria. The selective bacteriostatic (growth halting) properties of cationic AMPs are most often attributed to their ability to compromise bacterial membranes, while leaving eukaryotic cell membranes relatively unharmed. On entry into the periplasm or cytoplasm, various AMPs are known to interfere with cell wall growth, cause loss of osmotic pressure, and degrade the transmembrane potential (2, 3). It is increasingly clear that AMPs launch a multipronged attack on bacterial cells (4).

The hybrid antimicrobial peptide CM15 (KWKLFKKIGAVL-KVL-NH_2) combines residues 1–7 of cecropin A (from moth) with residues 2–9 of melittin (bee venom). CM15 retains the potency of cecropin A against multiple species of bacteria without the hemolytic activity of melittin (5). Using widefield fluorescence microscopy of plated *Escherichia coli* cells with excitation at 457 nm, we inadvertently discovered that addition of CM15 caused abrupt enhancement of cellular autofluorescence from the oxidized form of flavins. This led us to explore the possibility that CM15 induces harmful levels of reactive oxygen species (ROS) in the bacterial cytoplasm.

Our single-cell, real-time, fluorescence assays demonstrate that CM15 translocates across the outer membrane (OM) without permeabilization to periplasmic GFP, then permeabilizes the cytoplasmic membrane (CM) to GFP and causes abrupt cell shrinkage. Three different intracellular fluorescence signals indicate the onset of oxidative stress within 30 s of cell shrinkage: enhanced cytoplasmic autofluorescence from oxidized flavins, a burst of fluorescence from the permeable dye CellROX Green (CellROX product data sheet available on request) (known to detect O_2^- and •OH), and a burst of fluorescence from resorufin (the product of the Amplex Red assay, known to specifically detect H_2O_2). Additional tests suggest that components of the aerobic respiratory chain contribute to the CM15-induced ROS signals. Importantly, in anaerobic growth conditions the CellROX* (oxidized, fluorescent form of CellROX Green) and resorufin signals decrease significantly and the minimum inhibitory concentration (MIC) increases 20-fold. Oxidative stress is a key aspect of the growth-halting capability of CM15. This may prove true of many natural cationic AMPs, as suggested by our observation of a strong, abrupt CellROX* signal on attack of *E. coli* by the human cathelicidin LL-37.

Recent reports indicate that in addition to their target-specific action, bactericidal drugs such as norfloxacin, ampicillin, and kanamycin A induce oxidative stress in *E. coli* and *Staphylococcus aureus* (6, 7). Oxidative damage was evidently essential for complete killing of cells. The initial results have been challenged (8–10), and very recently these challenges have been refuted (11). Evidently, oxidative stress contributes to the lethality of a variety of antimicrobial agents (12, 13), including at least some antimicrobial peptides. The methods presented here enable detection of ROS within the cytoplasm of single cells with 12-s time resolution, a capability that should prove useful in many different contexts.

Results

Disruption of *E. coli* Membranes by CM15. We used previously developed single-cell, real-time imaging assays (14–16) to monitor the disruption of K12 *E. coli* membranes by CM15. The modified K12 cells include a plasmid to express GFP with the twin-arginine translocase signal peptide appended to the N terminus. GFP folds in the cytoplasm and is exported to the periplasm, where it is mobile (17). Cells are plated in a microfluidics chamber and are growing in continuously refreshed, aerated medium. On excitation at 488 nm, the resulting cells exhibit a halo of green fluorescence

Significance

Antimicrobial peptides (AMPs) help to kill invading bacteria on skin and lung surfaces. We are developing fluorescence microscopy assays that reveal the mechanisms of action of AMPs in real time. It is increasingly clear AMP damage to bacterial cells goes far beyond permeabilization of membranes. Here we demonstrate that for *Escherichia coli* in aerobic conditions, the peptide CM15 [combining residues 1–7 of cecropin A (from moth) with residues 2–9 of melittin (bee venom)], induces a burst of biochemically harmful reactive oxygen species within 30 s of membrane permeabilization. In anaerobic conditions, CM15 is 20-fold less potent. AMP efficacy in vivo may be tuned to the local level of oxygenation.

Author contributions: H.C. and J.C.W. designed research; H.C. and Z.Y. performed research; H.C. and J.C.W. analyzed data; and H.C. and J.C.W. wrote the paper.

The authors declare no conflict of interest.

This article is a PNAS Direct Submission.

[1]To whom correspondence should be addressed. Email: weisshaar@chem.wisc.edu.

This article contains supporting information online at www.pnas.org/lookup/suppl/doi:10.1073/pnas.1417703112/-/DCSupplemental.

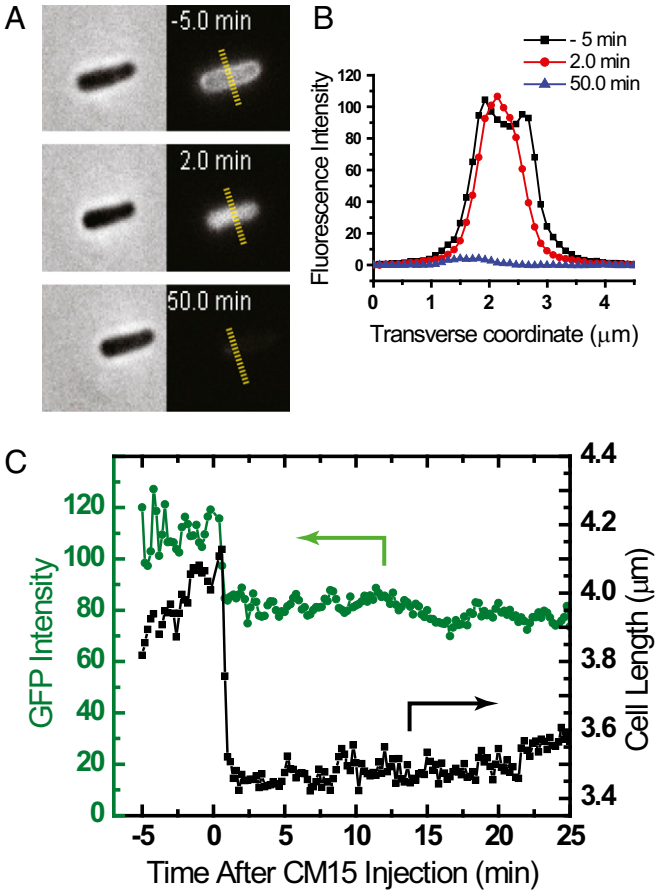

Fig. 1. Effects of 10 μM CM15 (twice the 6-h MIC) on MG1655 *E. coli* expressing periplasmic GFP. (*A*) Phase contrast and GFP fluorescence images of the same cell 5 min before, 2 min after, and 50 min after the onset of CM15 injection. (*B*) Transverse intensity linescans along the yellow hashed lines of *A*, showing periplasmic (−5 min), cytoplasmic (+2 min), and essentially absent (+50 min) GFP spatial distributions. (*C*) Single-cell time dependence of cell length (from phase contrast images) and total GFP fluorescence intensity before and after injection of 10 μM CM15. Cell length and GFP intensity decrease abruptly and simultaneously as GFP enters the cytoplasm. The decrease in GFP intensity is presumably due to the higher pH in the cytoplasm (14).

(Fig. 1), indicating a predominantly periplasmic spatial distribution of GFP. Fluorescence images are interleaved with phase contrast images that monitor cell length vs. time to a precision of ±50 nm. One full imaging cycle is completed every 12 s.

At $t = 0$, we initiate flow of 10 μM CM15 (twice the 6-h MIC, *SI Appendix*, Fig. S1) in EZ rich defined medium (EZRDM) medium through the microfluidics chamber and begin imaging single cells. For at least 85% of the cells in a typical field of 25 cells, within 12–24 s of CM15 injection, we observe abrupt shrinkage of the cell length and simultaneous migration of GFP from the periplasm into the cytoplasm (Movie S1). Similar events occur later for the remainder of cells. For one representative nonseptating cell, Fig. 1 *A* and *B* shows a phase contrast image and the transverse fluorescence intensity profile before and after the shrinkage event. Figure 1*C* shows the time evolution of total GFP fluorescence intensity and of tip-to-tip cell length. The inward movement of GFP implies rapid translocation of the peptide across the outer membrane (OM) without permeabilization to GFP, followed by permeabilization of the cytoplasmic membrane (CM) to GFP (16). Diffusive transfer of GFP to the cytoplasm is driven by the large cytoplasmic volume compared with the periplasmic volume. We suspect that cell shrinkage is due to leakage of small osmolytes across the CM and consequent loss of turgor pressure. Much later, at ∼30 min after cell shrinkage, each cell abruptly loses essentially all GFP fluorescence, indicating that the OM has also been permeabilized to GFP (Fig. 1*A*). Meanwhile, phase contrast is retained, showing that the chromosomal DNA and larger cytoplasmic components such as ribosomes are retained within the cell envelope.

Our subsequent studies of oxidative stress used wild-type K12 cells (not expressing GFP) to enable clean observation of signals from fluorescent probes of oxidative stress. At the same CM15 concentration of 10 μM, most wild-type cells exhibit cell shrinkage on a similarly rapid timescale of 12–24 s after injection of CM15. The moment of cell shrinkage observed in the phase contrast images serves as a nonfluorescent marker of the time of permeabilization of the CM to GFP, and presumably also to the much smaller CM15.

Enhancement of Cellular Autofluorescence by CM15 in Aerobic Conditions. The first probe of oxidative stress measures the intensity of cellular autofluorescence excited at 457 nm as a function of time after CM15 addition. At this excitation wavelength, the autofluorescence of *E. coli* is dominated by the oxidized forms of riboflavin (which is soluble) and flavin nucleotides (such as FAD and FMN). These share a common chromophore, which is nonfluorescent in its fully reduced form but becomes weakly fluorescent when fully oxidized (18). In Fig. 2*A*, we compare emission spectra from a solution of FAD and a suspension of K12 *E. coli*, both excited at 457 nm. The good agreement strongly

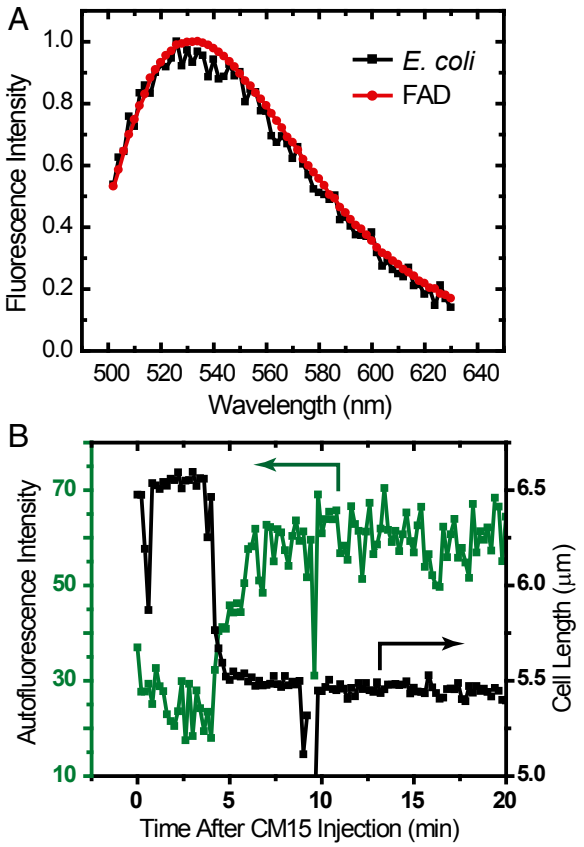

Fig. 2. (*A*) Comparison of emission spectra excited at 457 nm for an *E. coli* cell culture grown at 30 °C to OD_{600} ∼0.4 and a solution of 100 μM FAD. (*B*) Single-cell time dependence of cell length (from phase contrast images) and total autofluorescence (excited at 457 nm) before and after injection of 10 μM CM15.

suggests that flavin nucleotides and riboflavins are the source of cellular autofluorescence. The transverse spatial distribution is that of a filled cytoplasm, indicating that cellular autofluorescence is predominantly due to soluble flavins and flavin cofactors bound to soluble enzymes, not membrane-bound species.

Plots of total autofluorescence intensity and cell length vs. time for one representative cell are shown in Fig. 2*B*. The autofluorescence intensity begins to increase within 30 s of cell shrinkage. Evidently the cytoplasm has become more oxidizing. Over the next 2 min, the intensity rises to a plateau value two to three times as large as the pre-CM15 level. Before permeabilization of the cytoplasmic membrane by CM15, the autofluorescence decreases due to photobleaching. The broad plateau after CM15 action is likely due to a balance between photobleaching and continuing production of oxidized flavins and riboflavins. This same behavior was observed in all cells (typically at least 20) in each of five experiments.

Enhancement of CellROX Green Fluorescence by CM15 in Aerobic Conditions. The following single-cell, time-resolved tests attempt to dissect the oxidative stress induced by CM15 into contributions from enhanced production of the ROS superoxide (O_2^-), hydrogen peroxide (H_2O_2), and hydroxyl radical (•OH). In vitro, the permeable dye CellROX Green is oxidized by O_2^- and •OH, but not by H_2O_2. We call reduced CellROX Green "CellROX," and the fluorescent, oxidized form "CellROX*." As added, CellROX exhibits very weak fluorescence. In vitro, oxidation of CellROX by superoxide (presumably in its protonated •OOH form) or •OH induces strong CellROX* fluorescence (excited at 488 nm and detected at 525 ± 25 nm), but only in the presence of dsDNA, to which it must bind to fluoresce efficiently. In *SI Appendix*, Fig. S2, we describe in vitro tests that confirm that O_2^- in the presence of dsDNA can induce CellROX* fluorescence. The tests also show that the Fe^{2+} in either superoxide dismutase (SOD) or horseradish peroxidase (HRP) is unable to induce CellROX* fluorescence. In vitro, we observe no CellROX* fluorescence in the presence of 1 mM H_2O_2. To confirm that H_2O_2 itself cannot induce CellROX* fluorescence in vivo, we continuously flowed 10 μM H_2O_2 in PBS across plated K12 cells in the absence of CM15. No CellROX* fluorescence was observed (*SI Appendix*, Fig. S3). This also indicates that the ambient Fe^{2+} concentration is too low to drive sufficient •OH from Fenton chemistry quickly enough to produce observable CellROX* fluorescence (19).

We injected CM15 at 10 μM (twice the MIC) plus CellROX at 2.5 μM onto plated K12 cells at $t = 0$. As shown in Fig. 3*A*, strong CellROX* fluorescence begins to rise within 12 s of the abrupt cell shrinkage event (Movie S2). The CellROX* intensity peaks at ∼1 min later. Over the next 5 min, the signal decreases toward a plateau value. Evidently the fluorescent state CellROX* is being destroyed, perhaps by subsequent oxidative damage to the fluorophore; see below. The spatial distribution of the fluorescence intensity is that of the nucleoids, including well-separated primary nucleoid lobes and also secondary sublobes (Fig. 3*A*) (20). This pattern confirms binding of the oxidized, fluorescent CellROX* species to DNA. Similar events occurred in all 56 cells observed over 40 min in two separate experiments. Addition of CellROX alone (no CM15) gives only a smaller, slowly rising signal (Fig. 3*A*).

It was possible that CellROX was being oxidized in the bulk medium, entered the cell upon loss of membrane integrity, and became fluorescent on binding to DNA. We treated cells with 2% Triton X-100 (a nonionic detergent) plus 2.5 μM CellROX, without CM15. This treatment permeabilizes both *E. coli* membranes in ∼1 min. Over 40 min, cells showed very little CellROX* fluorescence (Fig. 3*D* and *SI Appendix*, Fig. S4).

We also tested for enhancement of CellROX* fluorescence at CM15 concentrations of half the MIC (2.5 μM) and 10 times the MIC (50 μM). The data are summarized in *SI Appendix*, Figs. S9 and S10). For CM15 at 2.5 μM, about 20% of cells shrank and then abruptly exhibited CellROX* fluorescence comparably strong to that induced at 10 μM. The remaining cells never shrank and continued to grow normally over the 30-min observation period. For CM15 at 50 μM, all cells exhibited strong CellROX* fluorescence much like induced at 10 μM. The lag times to cell shrinkage and the onset of CellROX* fluorescence were even shorter at 50 μM than at 10 μM.

Attenuation of CellROX* Fluorescence in Anaerobic Conditions. If CellROX is oxidized primarily by O_2^- and/or •OH, then addition of CM15 to cells growing anaerobically should induce less CellROX* fluorescence. In the following studies, cells grew in aerobic conditions for 150 min (enabling periplasmic GFP to become fluorescent) and then were plated and grew in anaerobic conditions for 30 min before observation. On addition of 10 μM CM15 (twice the aerobic MIC) to cells expressing periplasmic GFP, abrupt shrinkage occurred for all cells within 30 s. Subsequent events varied from cell to cell. About 25% of the cells showed behavior similar to that in aerobic conditions. Periplasmic GFP first migrated to the cytoplasm, and GFP was lost completely (permeabilization of the OM) only much later. Other behaviors include membrane blebbing, complete loss of GFP signal as the initial event, and formation of small "bubbles" containing GFP. A gallery of postshrinkage GFP fluorescence patterns is provided in *SI Appendix*, Fig. S5.

Next we added 10 μM CM15 plus 2.5 μM CellROX to wild-type K12 cells growing in the anaerobic chamber. Abrupt cell shrinkage again occurred within 30 s. For all 43 cells in two different experiments, we observed an abrupt but small increase in CellROX* signal beginning within 12 s of cell shrinkage (example in Fig. 3*B*). Comparing 11 well-isolated cells in aerobic conditions with 15-well isolated cells in anaerobic conditions, the average peak amplitude was at least five times smaller in anaerobic conditions (Fig. 3*D*). Evidently, oxygen is a prerequisite for induction of a strong CellROX* by CM15.

Importantly, the 6-h MIC of CM15 against K12 *E. coli* is 20-fold higher in anaerobic conditions (100 μM) than in aerobic conditions (5 μM) (*SI Appendix*, Fig. S1). This indicates that the oxidative stress induced by CM15 is an important factor in its bacteriostatic potency. Whereas we observed cell shrinkage and other membrane-altering effects of CM15 at 10 μM in anaerobic conditions, evidently some cells survive and reestablish growth. The fivefold decrease in CellROX* response in anaerobic conditions provides further evidence of ROS enhancement in aerobic conditions.

Below we will present evidence that the CM15-induced CellROX* signal observed in aerobic conditions depends on a functional respiratory electron transport chain. To test whether a different functional electron transport chain behaves similarly, we grew cells anaerobically in a constant flow of EZRDM medium supplemented with 10 mM KNO_3 for 30 min, and then injected 10 μM CM15 along with 2.5 μM CellROX and 10 mM KNO_3. Under these conditions, cells respire using nitrate reductase as the terminal complex (instead of cytochrome oxidase) and menaquinone as the membrane-bound electron carrier (instead of ubiquinone) (21). The resulting mean peak CellROX* signal was 12 times smaller than in aerobic conditions (Fig. 3*D*). We do not know how the flux of electrons compares between the anaerobic nitrate reduction pathway and the aerobic oxygen reduction pathway. However, the result suggests that some feature specific to the aerobic electron transport chain facilitates the strong CM15-induced CellROX* signal.

Effects of Cyanide and Azide Pretreatment in Aerobic Conditions. Cyanide (added as KCN) and azide (NaN_3) are known to inhibit heme-containing enzymes. In *E. coli*, these include the

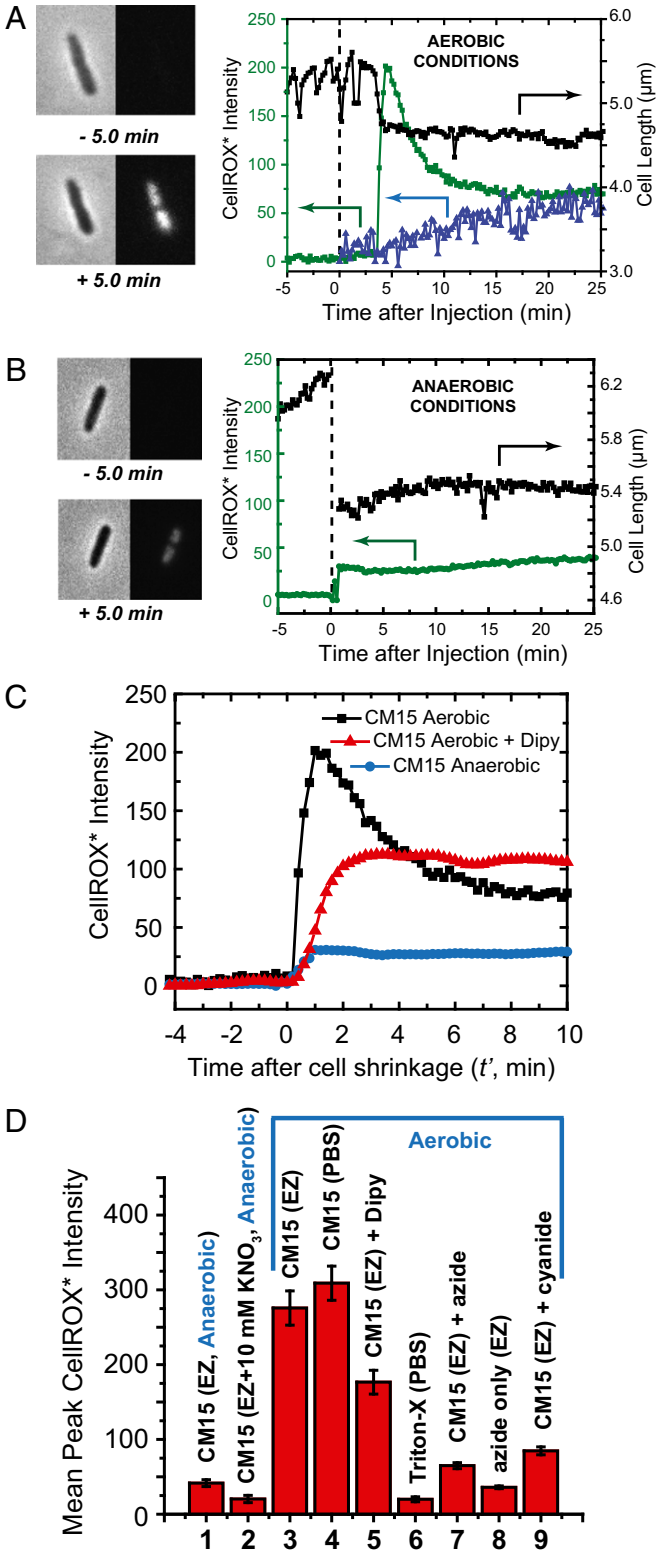

Fig. 3. CellROX* fluorescence and cell length measurements on addition of 10 μM CM15 in various conditions. (*A*) Aerobic growth conditions. (*Left*) Phase contrast and green fluorescence images before and after CM15 addition at $t = 0$. (*Right*) Time dependence of cell length (black) and total CellROX* fluorescence intensity (green) for the same cell. Blue data show CellROX* intensity vs. time for a different cell for which CellROX* alone (no CM15) flowed beginning at $t = 0$. (*B*) Anaerobic growth conditions. (*Left*) Phase contrast and green fluorescence images before and after CM15 addition at $t = 0$. (*Right*) Time dependence of cell length and total CellROX* fluorescence intensity. (*C*) Comparison of representative single-cell CellROX* fluorescence intensity traces after CM15 addition in aerobic conditions, in aerobic conditions with addition of 2,2′-dipyridyl (iron chelating agent), and in anaerobic conditions. (*D*) Bar graph of mean, single-cell CellROX* peak fluorescence intensity in nine different sets of experimental conditions. Error bars are ±1 SD of the mean in each condition. 1 and 2: Anaerobic conditions. CM15 addition to cells in standard EZRDM medium and in EZRDM supplemented with 10 mM KNO_3, respectively. 3–9: Aerobic conditions as follows. 3: CM15 addition to cells growing in EZRDM. 4: CM15 addition after rinsing cells with PBS to remove external iron. 5: CM15 addition in EZRDM to cells pretreated with 2,2′-dipyridyl to chelate free cytoplasmic iron. 6: No CM15; addition of 2% Triton-X in PBS. 7: CM15 addition to cells pretreated with 15 mM azide (NaN_3). 8: No CM15. Addition of 15 mM azide alone to cells growing in EZRDM. 9: CM15 addition to cells pretreated with 1 mM cyanide (NaCN). See text for additional details.

catalases, the peroxidases, and the terminal cytochrome oxidase complex, but not NADH dehydrogenase I and II (NDH-I and NDH-II) or the ubiquinones of the electron transport chain (22). In aerobic conditions, cytochrome oxidase carries out the four-electron transfer step converting O_2 to H_2O, simultaneously pumping protons across the CM to generate part of the proton-motive force (PMF) (19). Treatment of cells with either azide or cyanide degrades the PMF by inhibiting binding of O_2 to the catalytic site of cytochrome oxidase.

We pretreated plated K12 cells with 15 mM NaN_3 in EZRDM for 5 min, after which we initiated flow of medium containing CM15 at 10 μM plus CellROX at 2.5 μM. A small CellROX* signal begins to rise within 12 s of cell shrinkage, reaching a plateau that is fourfold smaller on average than for untreated cells (Fig. 3*D*). We also flowed NaN_3 plus CellROX (no CM15) over plated cells growing aerobically. We observed a very small CellROX* signal about half the magnitude of that induced by CM15 action on cells pretreated with azide (eightfold smaller than that induced by CM15 in untreated cells) (Fig. 3*D*). Similar results were observed for pretreatment with 1 mM KCN for 5 min followed by CM15 (Fig. 3*D*). Evidently, inhibition of aerobic respiration by pretreatment with azide or cyanide interferes with the mechanism by which CM15 induces CellROX* formation. In addition, inhibition of respiration by azide alone (no CM15) produces very little CellROX*.

Enhancement of Resorufin Fluorescence by CM15 in Aerobic Conditions. Next we adapted the well-established Amplex Red method (11, 23) for use as a single-cell, intracellular, time-resolved assay for H_2O_2 production following CM15 treatment. Some peroxidases catalyze reaction of the nonfluorescent species Amplex Red with H_2O_2 to form the fluorescent species resorufin (emission at 585 nm). Following Collins and coworkers (11), we carried out the Amplex Red + H_2O_2 reaction inside the cytoplasm by inserting a plasmid that expresses the nonnative peroxidase APEX2 (mutated ascorbate peroxidase). Unlike the catalases naturally occurring in *E. coli*, APEX2 is able to convert Amplex Red + H_2O_2 to resorufin. Intracellular detection of resorufin by fluorescence microscopy greatly improves the temporal and spatial resolution of the assay.

We repeated the flow experiment in aerobic conditions using the K12 strain expressing APEX2. At $t = 0$, we flowed 10 μM of CM15 plus Amplex Red at 10 μM. A strong burst of resorufin fluorescence begins to rise within 12 s of cell shrinkage (Fig. 4*A* and Movie S3). The signal peaks ~3 min after cell shrinkage and then partially decays over the next 20 min. All 23 observed cells exhibited similar behavior in aerobic conditions. In anaerobic conditions, there is little if any resorufin fluorescence after cell shrinkage (example in Fig. 4*B*); the mean peak signal is at least a factor of 50 smaller than in aerobic conditions.

For aerobic conditions, in Fig. 4*C* we compare the rising edge of resorufin signals averaged over five different cells with the

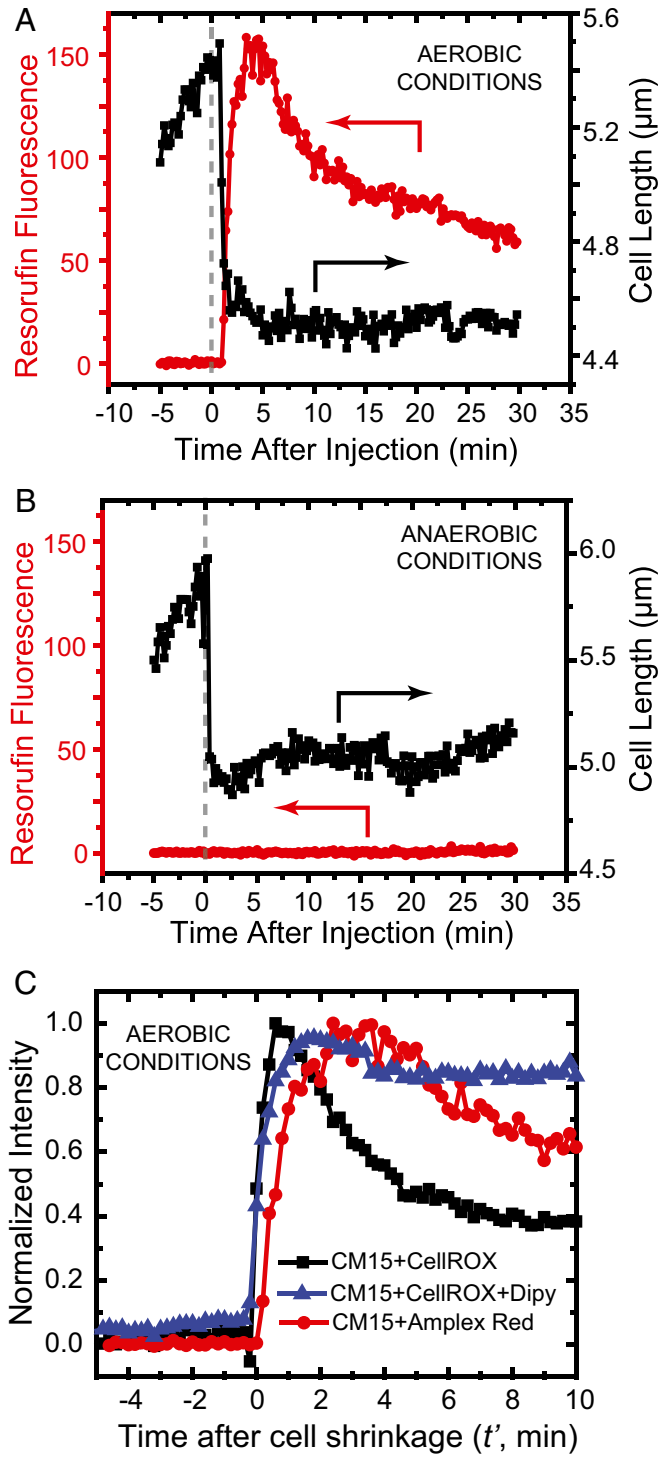

Fig. 4. Single-cell detection of H_2O_2 production following CM15 addition to cells expressing the nonnative peroxidase APEX2 from a plasmid. (*A*) Aerobic growth conditions. Single-cell measurement of resorufin fluorescence vs. time after addition of 10 μM CM15 at $t = 0$. Signal begins to rise within 12 s of cell shrinkage event. (*B*) Same as *A*, but for growth in anaerobic conditions. (*C*) Comparison of rising edge of CellROX* signal (with and without 2,2′-dipyridyl) and of resorufin signal after 10 μM CM15 treatment. Each trace is an average of five experiments, and the traces are normalized to the same peak intensity to facilitate comparisons. Time $t' = 0$ is the moment of cell shrinkage, used to place all cells on a common time axis.

rising edge of CellROX* signals (with and without pretreatment with 2,2′-dipyridyl; see below). To place all signals on the same time axis, the traces are plotted with $t' = 0$ defined as the time of abrupt cell shrinkage. All three averaged signals rise at very similar times relative to the cell shrinkage event. It is possible that the resorufin signal (presumably arising from H_2O_2) may lag the CellROX* signal (presumably from O_2^- and/or •OH) by one to two frames, or 12–24 s, but the different overall shapes of the two signals prevent a firm conclusion.

Effects of Chelation of Free Iron by 2,2′-Dipyridyl in Aerobic Conditions. Thus far, we have evidence of rapid, CM15-induced production of either O_2^- or •OH or both (from CellROX* fluorescence) and of H_2O_2 (from resorufin fluorescence) within 12–24 s of the cell shrinkage event. If CM15 were to cause a prompt burst of superoxide, at least part of the O_2^- would be rapidly converted to H_2O_2 by SOD. O_2^- may leach or destabilize solvent accessible Fe^{2+} within enzymes containing [4Fe–4S] clusters, such as dehydratases, and within mononuclear Fe-containing proteins as well (19). Thus, a prompt burst of O_2^- might quickly enhance both Fenton reactants ($H_2O_2 + Fe^{2+} \rightarrow$ •OH + $OH^- + Fe^{3+}$) and lead to a burst of •OH production (24).

The permeable iron chelating agent 2,2′-dipyridyl (here "dipyridyl") is known to efficiently chelate free iron (Fe^{2+}) and prevent Fenton chemistry in the cytoplasm (25). In an attempt to dissect the CellROX* signal into contributions from O_2^- (induced by CM15) and from •OH (formed by Fenton chemistry), we preincubated K12 cells for 5 min with 1 mM of dipyridyl. After plating the preincubated cells, we initiated continuous flow of 10 μM CM15 plus 2.5 μM CellROX plus 1 mM dipyridyl and measured CellROX* fluorescence vs. time. The signal begins to rise within 12 s of cell shrinkage and reaches a plateau ∼2 min later (example in Fig. 3*C*). The mean plateau value is about half of the mean peak level of CellROX* fluorescence without dipyridyl (Fig. 3*D*). In the presence of dipyridyl, the CellROX* signal maintains its plateau level over 10 min. Without dipyridyl, about half of the CellROX* signal decays over 5 min (Fig. 3*A*). Evidently dipyridyl prevents formation of part of the oxidants that form CellROX* and also all of the oxidants that degrade the CellROX* signal over 5 min in the absence of dipyridyl (comparison in Fig. 3*C*). The most likely oxidizing species in both cases is •OH.

The EZRDM growth medium contains 10 μM Fe^{2+} in the form of $FeSO_4$ salt, which might quickly enter the cytoplasm after permeabilization of the cytoplasmic membrane by CM15 and drive Fenton chemistry. To test this possibility, we plated cells, washed them in simple PBS solution to remove external iron, and then flowed in CM15 at 10 μM with CellROX at 2.5 μM, also in PBS. We observed a strong burst of CellROX* fluorescence immediately after cell shrinkage, with similar time dependence as in EZRDM (*SI Appendix*, Fig. S6).

Presumably the attenuation of CellROX* fluorescence by dipyridyl is due to chelation of internal free iron. These results are consistent with the hypothesis that CM15 induces formation of both O_2^- and •OH, each leading to about half of the peak CellROX* fluorescence intensity. This qualitative result does not imply that the peak concentrations of O_2^- and •OH are similar. Numerous competitive kinetic factors will influence the amount of CellROX* signal generated by O_2^- vs. •OH.

Discussion

The initial inward movement of periplasmic GFP caused by the short, cationic antimicrobial peptide CM15 contrasts sharply with the effects of the longer cationic, helical antimicrobial peptides LL-37 (16) and cecropin A (15). For those AMPs, the first observed effect was permeabilization of the OM to GFP, resulting in complete loss of GFP fluorescence. Several minutes later, the CM was permeabilized, as evidenced by entry into the cytoplasm of the DNA-staining dye Sytox Green. Facile trans-

location across the OM of *E. coli* by short cationic peptides may prove fairly general.

Taken together, the new time-resolved data provide strong evidence that in aerobic growth conditions, CM15 induces a burst of reactive oxygen species in the *E. coli* cytoplasm. Three independent fluorescence signals indicate the abrupt onset of oxidative stress within 30 s of the cell shrinkage event: enhancement of cellular autofluorescence (Fig. 2*B*), a burst of CellROX* fluorescence (Fig. 3*A*), and a burst of resorufin fluorescence from the Amplex Red/APEX2 assay (Fig. 4*A*). Studies in vitro show that CellROX Green detects both O_2^- and •OH, but does not detect H_2O_2 or the iron within SOD or HRP (*SI Appendix*, Fig. S2). The twofold attenuation of CellROX* fluorescence by the iron chelator 2,2′-dipyridyl (Fig. 3 *C* and *D*) implicates free Fe^{2+} and suggests appreciable formation of both O_2^- and •OH, the latter presumably from Fenton chemistry. The Amplex Red/APEX2 assay detects H_2O_2 by a specific enzymatic reaction. In anaerobic growth conditions, the CellROX* fluorescence is attenuated fivefold (Fig. 3 *B* and *D*), the resorufin fluorescence is attenuated at least 50-fold (Fig. 4*B*), and the MIC increases by a factor of 20. The anaerobic data confirm oxygen as an underlying effector of the strong signals in aerobic conditions, corroborate involvement of ROS, and demonstrate that aerobic conditions greatly enhance the growth-halting effects of CM15.

We can infer some features of the underlying mechanism by which CM15 induces ROS and rule out some possibilities. First, a normally functioning aerobic respiratory chain does not oxidize CellROX sufficiently to explain the burst of CellROX* fluorescence after CM15 addition. On addition of CellROX alone (without CM15), a CellROX* signal of only moderate amplitude rises slowly over tens of minutes (Fig. 3*A*). This may be due to oxidation of CellROX by the normal, background levels of O_2^- or •OH or by other ambient oxidants.

Second, the 12-s time resolution of our assays reveals that the burst of ROS induced by CM15 occurs very quickly. At 10 μM of CM15, the lag time between AMP addition and cell shrinkage is only 12–24 s (one to two camera frames). Both the CellROX* and the resorufin fluorescence signals rise abruptly within an additional 12–24 s of cell shrinkage (Fig. 4*C*). The response time is even shorter using 50 μM of CM15. This ∼30-s response time argues against a mechanism in which CM15 triggers a stress response, which leads to changes in the transcription/translation profile of the cell. Furthermore, the prompt "freezing" of local movement of a DNA locus (Movie S4) and of RNA polymerase diffusive motion (Movie S5 and *SI Appendix*, Fig. S8) suggests that CM15 probably impairs normal transcriptional activity on a similarly rapid timescale.

In *E. coli* respiring aerobically, an important source of O_2^- and H_2O_2 is "autoxidation." That is the accidental scavenging of an electron by O_2, typically from reduced flavins in the cytoplasm or from reduced flavin cofactors in the membrane-bound respiratory chain (19). The concentrations of ROS are kept low by SODs (which convert O_2^- to H_2O_2) and catalases (which convert H_2O_2 to H_2O).

The fourfold smaller CM15-induced CellROX* signal after pretreatment of cells with azide or cyanide (Fig. 3*D*) suggests that proper respiration is essential for most of the strong CM15-induced CellROX* fluorescence burst in aerobically growing cells. However, simple disruption of the flow of electrons through the respiratory chain and degradation of the protonmotive force by CM15 does not explain the strong burst of CellROX* fluorescence. If it did, we would expect treatment with azide or cyanide alone (which blocks respiration) to yield CellROX* fluorescence similar to that from treatment with CM15 alone. Instead, it is eightfold smaller.

CM15 interaction with the aerobic respiratory electron transport chain itself is appealing, because the chain is membrane bound. We know that CM15 strongly disrupts the cytoplasmic membrane, even to the point of permeabilization to periplasmic GFP. CM15 might interact with NDH-I, NDH-II, the respiratory ubiquinones (Fig. 5), or soluble, cytoplasmic flavins in a way that enhances the rate of autoxidation. However, the fourfold attenuation of CM15-induced CellROX* fluorescence after pretreatment with cyanide or azide tends to rule out enhanced autoxidation as the main source of ROS under treatment with CM15 alone. Both cyanide and azide block the initial O_2 binding site within cytochrome oxidase (Fig. 5), causing electrons to "pile up" in the respiratory electron transport chain (26). The NADH concentration increases, which in turn leads to larger concentrations of reduced flavins. Two of many documented examples are the flavin cofactor within the NDH-II complex (which is reduced by reaction with NADH) and free FAD (which is reduced by electron transfer from NADH catalyzed by flavin reductase). Imlay has shown that cyanide treatment leads to enhanced autoxidation of such reduced flavins, increasing the flux of O_2^- and H_2O_2 (19). Thus, pretreatment of cells with azide or cyanide should enhance the concentrations of these reduced flavins before the CM15 attack. If CM15 were further enhancing autoxidation of the reduced flavins, we would expect a larger burst of CellROX* fluorescence from the pretreated cells. Instead, it is fourfold smaller. The same argument applies to autoxidation of the electron transport carrier ubiquinone (Fig. 5). Pretreatment with cyanide or azide should also enhance the concentration of reduced ubiquinones UQH_2, but CM15-induced production of CellROX* fluorescence is reduced.

As an alternative to enhancement of autoxidation, we suggest that CM15 may interact with cytochrome oxidase-bo_3 (Fig. 5) to induce improper release of O_2^- from its initial binding site at the heme Fe^{2+} center. After all, transfer of one electron to form an Fe^{3+}–O–O^- complex is likely the first step in the four-electron reduction of O_2 to H_2O (27). This hypothesis is consistent with

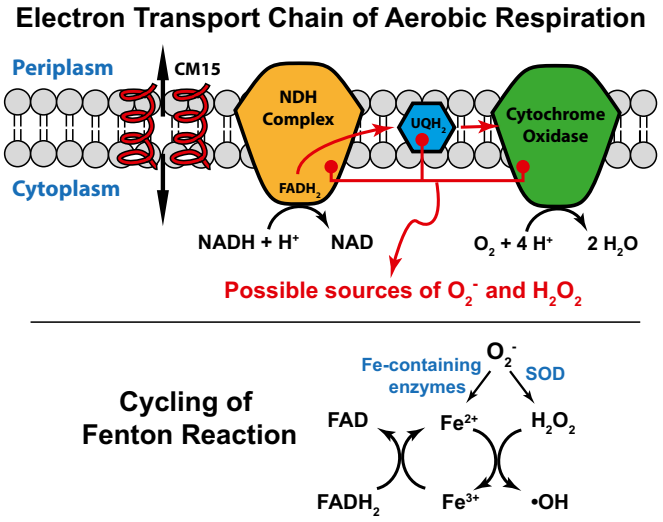

Fig. 5. (*Top*) Schematic of the aerobic respiratory electron transport chain in *E. coli*. Red arrows depict flow of electrons; black arrows depict chemical reactions. The NDH complex transfers electrons from NADH to ubiquinone (UQ) to form UQH_2. UQH_2 carries electrons to the terminal cytochrome oxidase-bo_3, which converts O_2 to H_2O in a four-electron reduction process. Helices depict CM15, which permeabilizes the cytoplasmic membrane seconds before the onset of oxidative stress. We suggest that CM15 induces premature release of O_2^- from cytochrome oxidase-bo_3. The data argue against a mechanism of enhanced autoxidation of the reduced flavin cofactor within NDH or of UQH_2. (*Bottom*) A burst of O_2^- enhances free Fe^{2+} by attacking Fe-containing enzymes and enhances H_2O_2 by the action of superoxide dismutase. This leads to cycling of the Fenton reaction, resulting in enhanced autofluorescence from oxidized flavin species (FAD) and further oxidation of CellROX Green.

the experimental fact that inhibition of O_2 binding to the heme by pretreatment with cyanide or azide decreases the CM15-induced CellROX* signal. Furthermore, CM15 addition to cells respiring anaerobically in nitrate-supplemented EZRDM induced a CellROX* signal 12 times smaller than that in aerobic conditions (Fig. 3*D*). The anaerobic chain uses the same NDH-I and NDH-II complexes as the aerobic chain and has similar electron carrier species (menaquinone instead of ubiquinone). The main difference is the terminal complex, which is nitrate reductase instead of cytochrome oxidase-bo_3 (21).

There is additional, indirect evidence supporting this hypothesis (28). A synthetic heme species was designed to mimic the catalytic function of cytochrome-*c* oxidase, the mitochondrial cytochrome oxidase, which is homologous to *E. coli* cytochrome-bo_3 complex. Proper coordination of the iron–porphyrin complex with a nearby copper center (mimicking Cu_B) and with a phenol group (mimicking Tyr^{244}) were essential to minimize release of partially reduced oxygen species, detected electrochemically as H_2O_2. Similarly, we suggest that CM15 perturbs cytochrome oxidase-bo_3, either by direct binding or indirectly by disrupting the local membrane structure, in a way that facilitates release of O_2^- from the complex. Future studies on *cyoC* deletion mutants and on inverted *E. coli* membranes will provide greater mechanistic insight.

Like CM15, the α-helical human cathelicidin LL-37 (37 aa, +7 net charge) also causes an abrupt increase in CellROX* fluorescence at the time of cell shrinkage (*SI Appendix*, Fig. S11). Evidently at least some natural antimicrobial peptides can induce oxidative stress in aerobically growing *E. coli*. The degree of oxygenation in different local environments in vivo might act to modulate AMP efficacy. For example, this might attenuate killing of *E. coli* in the gut but enable killing in more aerobic environments. The local environment also affects the potency of certain human defensins, whose efficacy is enhanced on reduction of the internal disulfide bonds (29).

There is recent additional evidence of oxidative damage by antimicrobial peptides, antimicrobial proteins, and even by standard small-molecule antibiotics. Expression of LL-37 from a plasmid in the *E. coli* cytoplasm led to enhanced fluorescence from the ROS reporter dye DCFH-DA, detected on a 2-h timescale (30). In both *Bacillus subtilis* and *E. coli*, the natural antibacterial agent peptidoglycan recognition protein (PGRP) enhanced fluorescence of the •OH reporter dye HPF, detected on a 1-h timescale (31). In *B. subtilis*, treatment with the synthetic peptide MP196 was shown to dislodge the electron carrier protein cytochrome-*c* (which plays the role of the *E. coli* ubiquinones) from the cytoplasmic membrane (4). Evidently, standard bactericidal drugs such as norfloxacin, ampicillin, and kanamycin also induce oxidative stress in the cytoplasm of strains of *E. coli* and *S. aureus* (6, 7, 11). For these drugs, metabolic perturbations leading to enhancement of ROS are a downstream consequence of the initial, specific antibiotic-target interactions (13).

Thus, it appears that oxidative stress is induced by a wide variety of antimicrobial agents, perhaps by different mechanisms in different cases. Single-cell fluorescence microscopy using permeable, oxidation-sensitive dyes provides a sensitive and selective means of measuring ROS formation in live bacterial cells with subminute time resolution. This enables correlation of the onset of ROS with other cellular events in real time. Previously developed assays carried out on bulk cultures lack such spatiotemporal resolution. In future work, we will apply these methods to a variety of AMPs and extend the scope to Gram positive species as well.

Materials and Methods

Bacterial Strains, Growth Conditions, and Materials. The background strain is MG1655 in all cases. For experiments on periplasmic GFP, TorA-GFP was expressed from a plasmid pJW1 as previously described (32). APEX2 was expressed using tetracycline in the same manner as TorA-GFP. The strain with *parS*-ParB-GFP labeling of the DNA locus called "Right2" was received from the Boccard laboratory (33).

Bulk cultures were grown in EZRDM (34), which contains a Mops-buffered solution with supplemented metal ions (M2130; Teknova), glucose (2 mg/mL), supplemental amino acids and vitamins (M2104; Teknova), nitrogenous bases (M2103; Teknova), 1.32 mM K_2HPO_4, and 76 mM NaCl. Cultures were grown from glycerol frozen stock to stationary phase overnight at 30 °C. Subcultures were grown to exponential phase (OD = 0.2–0.6 at 600 nm) before sampling for the microscopy experiments at 30 °C, unless otherwise specified.

We received *L*-CM15 with C-terminal amidation from Jimmy Feix (Medical College of Wisconsin, Milwaukee). The sequence is: KWKLFKKIGAVLKVL-NH_2. The oxidation sensitive dye CellROX Green (stock item no. C10444) and Amplex Red (A22188) was purchased from Invitrogen. Other chemicals are listed in detail in *SI Appendix*.

MIC Assay. The MIC for CM15 was determined using a broth microdilution method as previously described (16). Twofold serial dilutions of CM15 in 1× EZRDM were performed in separate rows of a polystyrene 96-well plate with each plate containing an inoculum of *E. coli* MG1655. The inoculum was a 1:20 dilution from a bulk culture at midlog phase (OD_{600} = 0.5) grown at 30 °C. The plate was incubated at 30 °C and shaken at 200 rpm in a Lab-Line Orbital Environ Shaker (model 3527) for 6 h for aerobic MIC measurements. The MIC values were taken as the lowest concentration for which no growth was discernible (<0.05 OD) after 6 h. The MIC value was 5 μM for *L*-CM15.

The anaerobic MIC was measured on a 96-well plate that was sealed with plastic wrap. Cells were incubated in EZRDM containing protocatechuic acid (PCA) at 10 mM and protocatechuate 3,4-dioxygenase (PCD) at 100 nM to scavenge oxygen (35). The plate was incubated at 30 °C for 6 h, followed by OD measurements. We tested that PCA by itself does not interfere with the CM15-induced burst of CellROX* fluorescence (*SI Appendix*, Fig. S7).

Microfluidics Chamber for Aerobic and Anaerobic Measurements. Imaging of individual cells was carried out at 30 °C in a simple microfluidics chamber consisting of a single rectilinear channel of uniform height of 50 μm and width of 6 mm, with a channel length of 11 mm. The total chamber volume is ∼10 μL. The negative of the cell design was patterned onto a silicon wafer via photolithography and the wafer was silanized. Sylgard 184 silicone elastomer mixture (Dow Corning) was poured onto the patterned silicon wafer and baked for 24 h in a 37 °C incubator after removing air in a vacuum desiccator. The cured polydimethylsiloxane (PDMS) slab was removed and holes were punched for entry and exit hypodermic needles. The patterned PDMS slab was fused to a dried, acetone-cleaned, 22-mm × 40-mm glass coverslip precleaned by plasma oxidation. Soon after the bonding of the two pieces, 0.01% poly-*L*-lysine (molecular weight >150,000 Da) was injected through the chamber for 30 min and rinsed thoroughly with Millipore water. For imaging experiments, the chamber was maintained at 30 °C with a TC-344B dual automatic temperature controller through the CC-28 cable assembly attached to RH-2 heater blocks (Warner Instruments).

The PDMS ceiling of the microfluidics device is permeable to the ambient gases N_2 and O_2. For anaerobic imaging experiments, we needed to prevent O_2 from entering the chamber through its ceiling. A small anaerobic chamber surrounding the microfluidics device was constructed of aluminum with a nitrogen gas inlet and outlet. Before injection of cells, nitrogen gas flowed through the chamber continuously for 1.5 h. *E. coli* were grown in aerobic conditions until injected into the chamber. Fresh deoxygenated EZRDM was made by treating EZRDM with 50 nM PCD and 2.5 mM PCA. This was used to wash the cells at 30 °C before plating. Deoxygenated EZRDM then flowed across the plated cells for 30 min before injection of CM15 and CellROX. The subsequent microscopy imaging experiment was carried out as before.

Microscopy. Single-cell imaging was performed on two different microscopes: a Nikon TE300 inverted microscope with a 100×, 1.3 N.A. phase contrast objective (Nikon) and Nikon Eclipse Ti inverted microscope with a 100×, 1.45 N.A. phase contrast objective (Nikon). For the Nikon TE300, images were further magnified 1.45× in a home-built magnification box. A line tunable Ar^+ laser (Melles Griot) at 488 nm or 457 nm was expanded to illuminate the field of view uniformly. Laser intensities at the sample were ∼10 W/cm^2 at 457 nm and ∼5 W/cm^2 at 488 nm. Fluorescence images were obtained with an EMCCD camera, either Andor iXon 897 or Andor iXon 887. In both cases, the pixel size corresponds to 110 ± 10 nm at the sample.

All emission filters were purchased from Chroma Technology. Specific emission filters were: 495LP (long-pass) for observation of autofluorescence after 457-nm excitation and HQ525/50 for observation of GFP or CellROX after 488-nm excitation and HQ617/70 for resorufin after 561-nm excitation.

Unless otherwise noted, time-lapse movies of 60-min total duration were obtained as 600 frames of 50-ms exposure time each, with fluorescence and phase contrast images interleaved at 6-s intervals (12 s per complete cycle). A movie begins immediately after adhesion of cells and the rinsing away of extra cells. The cells were imaged for ~5 min before injection of fresh medium containing the compounds under study (CM15, CellROX, etc).

Measurement of Single-Cell Autofluorescence. To obtain the fluorescence spectrum of normal MG1655 autofluorescence (Fig. 2), a cell culture grown at 30 °C to OD_{600} ~0.4 was sampled onto a black 96-well plate. The emission spectrum was obtained using a Tecan Infinite M1000 fluorimeter with excitation at 457 nm. For comparison, the fluorescence spectrum of 100 μM FAD was obtained under the same instrumental conditions (Fig. 3*A*).

For the single-cell autofluorescence measurements under the microscope, cells were excited by the Ar^+ laser at 457 nm after passage through a notch filter (Z458/10×) to eliminate plasma radiation. The emission through filter HQ525/50 was imaged. Movies were initiated ~5 min before changing the flow from normal aerated growth medium to aerated growth medium containing CM15 at 10 μM or H_2O_2 at 10 μM. For comparisons of autofluorescence intensity under different treatments, the laser intensity and camera gain were kept constant.

CellROX Green Oxidation Assay. CellROX Green is a proprietary oxidation-sensitive dye whose fluorescence quantum yield at 500–550 nm after excitation at 488 nm increases dramatically on oxidation in the presence of dsDNA. It readily permeates both *E. coli* membranes. The manufacturer tested its sensitivity to different reactive oxygen species in the presence of dsDNA in vitro including hydroxyl radical (•OH), superoxide (O_2^-), hydrogen peroxide (H_2O_2), peroxynitrite ($ONOO^-$), nitric oxide (NO), and hypochlorite (ClO^-). The only two oxidizing agents that significantly enhanced CellROX fluorescence were hydroxyl radical and superoxide. Importantly, hydrogen peroxide has no effect.

In the basic CellROX* imaging experiments, MG1655 cells were injected into the microfluidics chamber. After allowing 5 min for plating of cells, the bulk solution was washed away with fresh, prewarmed, aerated EZRDM. After the wash, cells were grown for 5 min before the injection of 10 μM CM15 with 2.5 μM CellROX. CellROX fluorescence after 488-nm excitation was monitored through emission filter HQ525/50. The laser intensity at the sample was ~2.5 W/cm^2. To maintain good aeration and steady bulk concentrations, the medium with CM15 and CellROX flowed continuously at 0.3 mL/h.

In attempts to intercept cycling of the Fenton reaction by chelating available cytoplasmic iron, cells were incubated in 1 mM of 2,2′-dipyridyl for 5 min after plating and before the injection of CM15.

Amplex Red Oxidation Assay. The assay for single-cell, time-resolved measurement of H_2O_2 production following CM15 treatment is based on the well established Amplex Red method (11, 23). Some peroxidases (not the catalases naturally occurring in *E. coli*) catalyze reaction of the dye Amplex Red with H_2O_2 to form the fluorescent species resorufin (λ_{em} = 585 nm). To measure the rate of H_2O_2 production under normal metabolism, Imlay and coworkers (36) studied an HPX^- mutant strain of *E. coli* (lacking catalase). The permeable H_2O_2 escapes the cell and undergoes a bulk reaction with Amplex Red, catalyzed by HRP. The product is resorufin, which absorbs at 570 nm and fluoresces strongly at 585 nm. The time resolution of this method was ~5 min. Recently Collins and coworkers (11) adapted the method to carry out the Amplex Red + H_2O_2 reaction inside the cytoplasm by inserting a plasmid that expresses the peroxidase APEX2 (mutated ascorbate peroxidase) into the cytoplasm. This method detects H_2O_2 production inside the cell using plate-based fluorescence measurements carried out with time resolution of ~60 min. Here we use intracellular APEX2 combined with single-cell, time-resolved detection by fluorescence microscopy, including a microfluidics chamber and an EMCCD camera. This enables sensitive detection of intracellular H_2O_2 production with 12-s time resolution and correlation of the CM15-induced H_2O_2 production with other events in real time.

ACKNOWLEDGMENTS. We thank Prof. Jimmy Feix (Medical College of Wisconsin) for providing CM15 samples and Dr. Piercen Oliver of the Weibel laboratory for guidance in construction of the microfluidic device. Profs. Tricia Kiley (University of Wisconsin-Madison, Department of Bacteriology) and James Imlay (University of Illinois at Urbana-Champaign, Department of Microbiology) were tremendously helpful in discussions of oxidative stress mechanisms.This work was supported by the National Institutes of Health (National Institute of General Medical Sciences, R01-GM094510 (to J.C.W.) and R01-GM093265 (to J.C.W. and Samuel H. Gellman).

1. Wimley WC, Hristova K (2011) Antimicrobial peptides: Successes, challenges and unanswered questions. *J Membr Biol* 239(1-2):27–34.
2. Brogden KA (2005) Antimicrobial peptides: Pore formers or metabolic inhibitors in bacteria? *Nat Rev Microbiol* 3(3):238–250.
3. Hancock RE, Sahl HG (2013) New strategies and compounds for anti-infective treatment. *Curr Opin Microbiol* 16(5):519–521.
4. Wenzel M, et al. (2014) Small cationic antimicrobial peptides delocalize peripheral membrane proteins. *Proc Natl Acad Sci USA* 111(14):E1409–E1418.
5. Schlamadinger DE, Wang Y, McCammon JA, Kim JE (2012) Spectroscopic and computational study of melittin, cecropin A, and the hybrid peptide CM15. *J Phys Chem B* 116(35):10600–10608.
6. Kohanski MA, Dwyer DJ, Hayete B, Lawrence CA, Collins JJ (2007) A common mechanism of cellular death induced by bactericidal antibiotics. *Cell* 130(5):797–810.
7. Kohanski MA, Dwyer DJ, Collins JJ (2010) How antibiotics kill bacteria: From targets to networks. *Nat Rev Microbiol* 8(6):423–435.
8. Liu Y, Imlay JA (2013) Cell death from antibiotics without the involvement of reactive oxygen species. *Science* 339(6124):1210–1213.
9. Keren I, Wu Y, Inocencio J, Mulcahy LR, Lewis K (2013) Killing by bactericidal antibiotics does not depend on reactive oxygen species. *Science* 339(6124):1213–1216.
10. Ezraty B, et al. (2013) Fe-S cluster biosynthesis controls uptake of aminoglycosides in a ROS-less death pathway. *Science* 340(6140):1583–1587.
11. Dwyer DJ, et al. (2014) Antibiotics induce redox-related physiological alterations as part of their lethality. *Proc Natl Acad Sci USA* 111(20):E2100–E2109.
12. Zhao X, Drlica K (2014) Reactive oxygen species and the bacterial response to lethal stress. *Curr Opin Microbiol* 21C:1–6.
13. Dwyer DJ, Collins JJ, Walker GC (2015) Unraveling the physiological complexities of antibiotic lethality. *Annu Rev Pharmacol Toxicol*, 10.1146/annurev-pharmtox-010814-124712.
14. Barns KJ, Weisshaar JC (2013) Real-time attack of LL-37 on single *Bacillus subtilis* cells. *Biochim Biophys Acta* 1828(6):1511–1520.
15. Rangarajan N, Bakshi S, Weisshaar JC (2013) Localized permeabilization of *E. coli* membranes by the antimicrobial peptide Cecropin A. *Biochemistry* 52(38):6584–6594.
16. Sochacki KA, Barns KJ, Bucki R, Weisshaar JC (2011) Real-time attack on single *Escherichia coli* cells by the human antimicrobial peptide LL-37. *Proc Natl Acad Sci USA* 108(16):E77–E81.
17. Sargent F (2007) The twin-arginine transport system: Moving folded proteins across membranes. *Biochem Soc Trans* 35(Pt 5):835–847.
18. Lu HP, Xun L, Xie XS (1998) Single-molecule enzymatic dynamics. *Science* 282(5395):1877–1882.
19. Imlay JA (2013) The molecular mechanisms and physiological consequences of oxidative stress: Lessons from a model bacterium. *Nat Rev Microbiol* 11(7):443–454.
20. Bakshi S, Siryaporn A, Goulian M, Weisshaar JC (2012) Superresolution imaging of ribosomes and RNA polymerase in live *Escherichia coli* cells. *Mol Microbiol* 85(1):21–38.
21. Unden G, Bongaerts J (1997) Alternative respiratory pathways of *Escherichia coli*: Energetics and transcriptional regulation in response to electron acceptors. *Biochim Biophys Acta* 1320(3):217–234.
22. Woodmansee AN, Imlay JA (2003) A mechanism by which nitric oxide accelerates the rate of oxidative DNA damage in *Escherichia coli*. *Mol Microbiol* 49(1):11–22.
23. Martell JD, et al. (2012) Engineered ascorbate peroxidase as a genetically encoded reporter for electron microscopy. *Nat Biotechnol* 30(11):1143–1148.
24. Flint DH, Tuminello JF, Emptage MH (1993) The inactivation of Fe-S cluster containing hydro-lyases by superoxide. *J Biol Chem* 268(30):22369–22376.
25. Imlay JA, Chin SM, Linn S (1988) Toxic DNA damage by hydrogen peroxide through the Fenton reaction *in vivo* and *in vitro*. *Science* 240(4852):640–642.
26. Messner KR, Imlay JA (2002) Mechanism of superoxide and hydrogen peroxide formation by fumarate reductase, succinate dehydrogenase, and aspartate oxidase. *J Biol Chem* 277(45):42563–42571.
27. Yoshikawa S, Muramoto K, Shinzawa-Itoh K (2011) Proton-pumping mechanism of cytochrome c oxidase. *Ann Rev Biophys* 40:205–223.
28. Collman JP, et al. (2007) A cytochrome *C* oxidase model catalyzes oxygen to water reduction under rate-limiting electron flux. *Science* 315(5818):1565–1568.
29. Schroeder BO, et al. (2011) Reduction of disulphide bonds unmasks potent antimicrobial activity of human β-defensin 1. *Nature* 469(7330):419–423.
30. Liu W, et al. (2013) Effect of intracellular expression of antimicrobial peptide LL-37 on growth of *Escherichia coli* strain TOP10 under aerobic and anaerobic conditions. *Antimicrob Agents Chemother* 57(10):4707–4716.
31. Kashyap DR, et al. (2014) Peptidoglycan recognition proteins kill bacteria by inducing oxidative, thiol, and metal stress. *PLoS Pathog* 10(7):e1004280.
32. Sochacki KA, Shkel IA, Record MT, Weisshaar JC (2011) Protein diffusion in the periplasm of *E. coli* under osmotic stress. *Biophys J* 100(1):22–31.
33. Thiel A, Valens M, Vallet-Gely I, Espéli O, Boccard F (2012) Long-range chromosome organization in *E. coli*: A site-specific system isolates the *Ter* macrodomain. *PLoS Genet* 8(4):e1002672.
34. Neidhardt FC, Bloch PL, Smith DF (1974) Culture medium for enterobacteria. *J Bacteriol* 119(3):736–747.
35. Aitken CE, Marshall RA, Puglisi JD (2008) An oxygen scavenging system for improvement of dye stability in single-molecule fluorescence experiments. *Biophys J* 94(5):1826–1835.
36. Park S, You X, Imlay JA (2005) Substantial DNA damage from submicromolar intracellular hydrogen peroxide detected in Hpx- mutants of Escherichia coli. *Proc Natl Acad Sci USA* 102(26):9317–9322.